

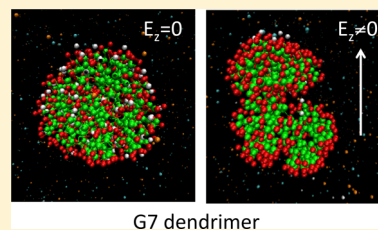
Charged Dendrimers in Trivalent Salt Solutions under the Action of DC Electric Fields

Ashok K. Das and Pai-Yi Hsiao*

Department of Engineering and System Science, National Tsing Hua University, Hsinchu, 30013, Taiwan, R. O. C.

S Supporting Information

ABSTRACT: The structural properties and electrophoretic mobility of charged dendrimers in 3:1 electrolyte solutions subjected to direct current electric fields are studied using molecular dynamics simulations. The simulated dendrimer size is studied in zero fields and found to scale as $R_g \sim N^{0.29}$. The dendrimers exhibit shape distortions when the applied electric field is larger than some critical value, which scales with the number of dendrimer monomers as $E_{z,crit} \sim N^{0.39(6)}$. Families of curves, such as the curves of the square of radius of gyration, the asphericity, the degree of prolateness, and the electrophoretic mobility of dendrimers, are shown to collapse to single, master curves in electric fields through appropriate scaling. This reflects the fractal characteristics of these systems. The density profile of the surface monomers and salt cations reveals two pronounced combination effects between the polarization of dendrimer complexes and stripping-off of the condensed salt cations from the dendrimer surface.



1. INTRODUCTION

Experimental separation and characterization of biomolecules, such as proteins, nucleic acids, bacteria, and viruses, rely heavily on the electrokinetic behavior of these molecules in applied electric fields. Techniques related to electrokinetics include electrophoresis and dielectrophoresis.¹ Recently, these techniques have been successfully exploited in nanofluidic devices, which hold promise for many applications such as controlled drug delivery,² gene therapy,³ and DNA sequencing.⁴

In this article, we investigate the behavior of dendrimers in applied electric fields. The spherical architecture of highly branched dendrimer molecules has been the subject of much attention for decades.^{5–8} The terminal units of dendrimers can be modified into various functional groups, leading to many novel nanomaterials.⁹ Such dendrimers have been used as heterogeneous catalysts, chemical sensors, biological sensors, contrast agents for magnetic resonance imaging, and transfection agents.¹⁰ Dendrimer-encapsulated nanoparticles have been used in homogeneous catalytic reactions in water, in supercritical CO₂, and in organic solvents.¹¹ Conjugates prepared from specific dendrimers and β -cyclodextrin have been shown to exhibit unique features in multidisciplinary fields, from gene delivery to host–guest recognition.¹² Dendrimers have a promising future in disease treatment, since they can be utilized to encapsulate drug molecules, which can then be driven in bloodstreams.^{13–15} In practice, the size of drug molecules should conform to the size of the vacuole in the carrier dendrimers. Furthermore, the presence of electrolytes in solution plays an important role in assisting the migration of the drug-encapsulated dendrimers in applied voltages. Recently, poly(amido amine) dendrimers (or briefly PAMAM dendrimers) and their derivatives have been studied with respect to their various medicinal and biomedical applications.^{16–18}

The structural properties of dendrimers in solutions depend on many factors such as the generation number n , the total number of monomers N , the spacer length s , and the nature of terminal groups.¹⁹ Early investigations by de Gennes and Hervet using a self-consistent theory²⁰ predicted that the radius of gyration of dendrimers scales as $R_g \sim N^{0.2} s^{0.4}$. Flory-type mean-field analysis suggests that this scaling is valid under good solvent conditions, while in poor solvents the scaling should change to $R_g \sim N^{1/3}$.^{8,21,22} Simulation studies of the scaling relation were first done by Lescanec and Muthukumar in 1990 using a kinetic-growth algorithm.²³ The scaling relation $R_g \sim N^{0.22} s^{0.5}$ was found. Murat and Grest²⁴ later performed molecular dynamics (MD) simulations and obtained the scaling relation $R_g \sim N^{1/3}$. Since then many efforts have been made using different simulation methods, such as MD,^{24,38–44} Monte Carlo (MC),^{8,21,22,25–37} and various coarse-grained^{37,38,42,43} and all-atom models,^{24,39–41} under different solvent conditions.^{8,24,26,28,29,36} Different scaling behaviors were obtained, and the claimed scaling exponent for N lies mainly between 0.2 and 0.35. Readers can refer to Table 1 of ref 36 for a list of the results and comparison. Experiments using holographic relaxation spectroscopy (HRS),⁴⁵ SANS,^{37,46} SAXS,⁴⁷ rheometry,⁴⁸ etc., support this range of scaling relations under various solvent conditions.

Temperature^{48,49} and pH value of solution^{46,50–52} also show important effects on the properties of dendrimers. For example, PAMAM dendrimers are partially charged in neutral solutions through the protonation of the surface terminal groups while fully charged in low-pH solutions through the protonation of both terminal and interior branching groups.⁵¹ Significant back-

Received: November 27, 2013

Revised: May 14, 2014

folding of dendrimers' outer-shell and water penetration within dendrimers are observed under different pH conditions, from MD simulations using all-atom models.⁴² MC simulations^{34,35} reveal that counterion condensation occurs mainly in the interior of dendrimers under low and neutral pH conditions. The dissociation of the condensed counterions into surrounding solutions gives rise to a nonmonotonous electrostatic swelling of the dendrimer with temperature. It is found that decreasing pH value leads to higher electrostatic swelling and stronger spacer-length dependence on dendrimer size.^{53,54}

Surface modification by ionizable functionality is another way to charge dendrimers in solutions.^{47,55–57} For example, sodium carboxylate-terminated Tomalia-type dendrimers dissociate into polyanions in aqueous solutions and form certain structural order even at low concentration, a result that depends on the effective charge interactions and solution conditions.⁴⁷ Varying the ionic strength of a solution by adding salt can significantly modulate the properties of charged dendrimers.^{58–60} A reversible transition from a “dense core” to a “dense shell” structure has been revealed by MC simulations,⁶⁰ as the ionic strength is cycled from high to low. The valence of the added salt plays a key role in determining dendrimer conformation.^{42,43} Increasing multivalent salt concentration in solutions can lead to a reduction of dendrimer size due to a drop of osmotic pressure inside the molecules, followed by a weak swelling due to an enhanced excluded volume effect of the adsorbed salt ions. Overcharging of dendrimers has been observed in multivalent salt solutions of high concentrations but has not been observed in monovalent salt solutions.⁴⁴

Capillary electrophoresis (CE) is used extensively to analyze the complexity of dendrimers.^{61–65} Shi et al. performed CE investigation of surface-modified polyanionic dendrimers.⁶⁵ Smaller electrophoretic mobility was found for the dendrimers with higher generation number, which can be attributed to the lower charge/mass ratio. For polycationic dendrimers, the mobility dependence on generation number was weaker due to the dominated interaction between the dendrimers and the capillary wall.⁶² Seyrek et al. investigated the effect of electric field on carboxyl-terminated dendrimers.⁵⁵ They found that the electrophoretic mobility increases with field strength in solutions of moderate ionic strength. At low ionic strength, the surrounding ion atmosphere drags the dendrimers, resulting in a decrease of the mobility.

In addition to the electrokinetic behavior, applying electric fields can alter the structure of dendrimers and the ionic distribution surrounding the molecules. Several works have been devoted to understanding these variations for linear polyelectrolyte systems. Using the results of Brownian dynamics simulations on collapsed linear polyelectrolytes, Netz has found that an unfolding transition occurs in high electric fields causing polyelectrolytes to align parallel to the external field.^{66,67} The critical field strength (E^*) exhibits a scaling relation $E^* \sim N^{0.5}$ with the chain length N . Various aspects of the unfolding behavior of polyelectrolyte in electric fields have also been investigated by other authors.^{68–77} However, equivalent studies for dendrimer systems remain scarce. In strong electric fields, conformational changes of charged dendrimers are expected due to polarization effects. For example, structural distortion, orientation alignment along the field direction, and redistribution of ions surrounding the dendrimers are all likely to occur. The electrophoretic mobility should also be significantly affected, due to changes of

dendrimer size and effective charge. These issues need to be examined thoroughly and are crucial in developing dendrimer-based nanodevices and gaining effective control for wider applications.

In this work, we investigate the orientation, shape distortion, and mobility of charged dendrimers in electric fields, through coarse-grained MD simulations, by varying the generation number. Important properties studied include the principal eigenvalue (λ_1) of the radius of gyration tensor, square of the radius of gyration (R_g^2), asphericity (A), degree of prolateness (P), and electrophoretic mobility (μ). Each of these properties follows a universal scaling behavior in varying electric fields. In section 2, we will describe our coarse-grained model and the simulation strategy. The results and discussion section (section 3) will then examine the importance of critical field strength requirement for each generation of the dendrimer. The orientation of the dendrimers in the presence of an electric field will be analyzed on the basis of the polarization phenomenon due to the surface charges and added salt cations. The radial density distributions of the surface monomers and salt cations, as well as the surface monomer–salt cation pair correlation function, demonstrate the stripping-off effect of the salt cations by the applied electric field. In the conclusion (section 4), we will summarize the important findings of our investigation and propose subsequent studies, which are worth pursuing.

2. MODEL AND SIMULATION METHOD

In order to reduce the computational cost, we use a coarse-grained model to study the behavior of charged dendrimers in DC electric fields. In this model, a monomer typically represents a fundamental group, such as $>N(CH_2)_2NHCO-(CH_2)_2N<$, in PAMAM dendrimers. A dendrimer is created iteratively from a “core”, generation by generation. For convenience, we will call the core of the dendrimer the zeroth generation (labeled G0). To create a dendrimer of generation n (denoted Gn), we attach two monomers to each monomer on the outer shell of the $G(n-1)$ dendrimer. Figure 1 presents the first few generations illustrating the definition of the core, inner monomers, and outer (surface) monomers. A Gn dendrimer comprises $N = 2^{n+3} - 2$ monomers, of which $N_s = 2^{n+2}$ monomers are located on the outer shell of the dendrimer and the rest reside in the inner shells. We assume that the inner monomers are charge-neutral while the outer monomers (also called surface monomers) carry charges, each one a $-e$ charge. It models carboxyl-terminated Tomalia-type dendrimers in aqueous solutions.⁵⁵ To maintain electroneutrality, a Gn dendrimer molecule dissociates 2^{n+2} monovalent cations (or counterions) into solutions.

As is well-known, the presence of multivalent electrolytes can strongly affect the structure and behavior of macromolecules in a solution.^{44,78–81} We add (3:1)-salt into the solutions where the salt molecules dissociate into trivalent cations and monovalent anions. We study the system near the stoichiometric point; i.e., the net total charge of the added trivalent cations can neutralize the total charge on the dendrimer. The solvent is modeled implicitly as a dielectric medium.

The excluded volume interaction is applied to any pair of particles, including the monomers and the ions. It is modeled using the truncated Lennard-Jones (LJ) potential function^{82,83}

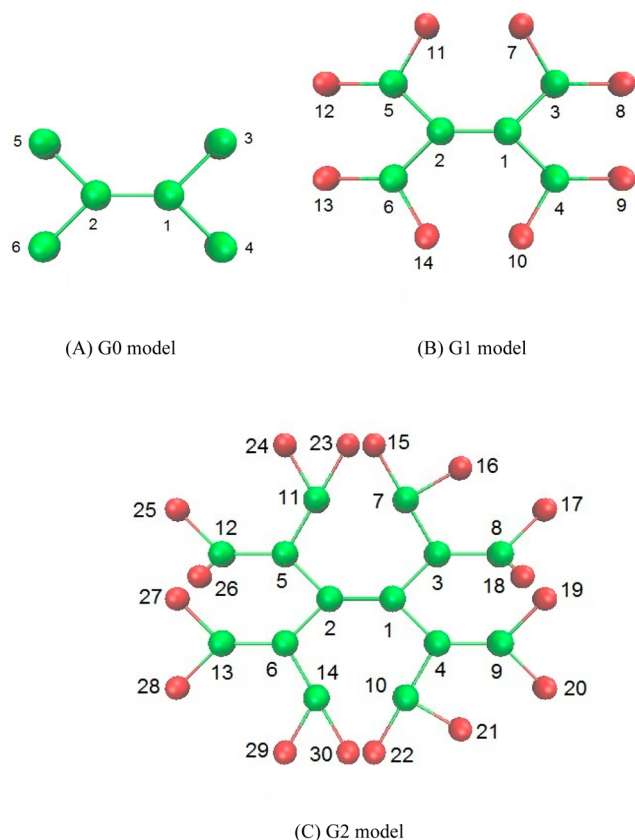


Figure 1. Illustration of the coarse-grained models of dendrimers: (A) G0 model, (B) G1 model, (C) G2 model. Each sphere is a monomer representing a group of atoms. Monomer Nos. 1–6 form the “core”. Green spheres represent the inner monomers, while the red ones represent the outer monomers. Lines connecting the spheres are the FENE bonds (see text).

$$U_{\text{LJ}}(r_{ij}) = \begin{cases} 4\epsilon \left[\left(\frac{\sigma}{r_{ij}} \right)^{12} - \left(\frac{\sigma}{r_{ij}} \right)^6 \right] + \epsilon & r_{ij} \leq (2)^{1/6} \sigma \\ 0 & r_{ij} > (2)^{1/6} \sigma \end{cases} \quad (1)$$

where r_{ij} is the distance between the two interaction sites and ϵ and σ are the LJ energy and distance parameters, respectively. For simplicity, we assume that ϵ and σ are identical for all the particles.

Interactions among the charged species in the system (including surface monomers, counterions, salt cations, and salt anions) are defined in terms of the Coulomb potential

$$U_{\text{Coul}}(r_{ij}) = k_{\text{B}} T Z_i Z_j \frac{\lambda_{\text{B}}}{r_{ij}} \quad (2)$$

where Z_i and Z_j are the valences carried on the two sites, respectively; k_{B} is the Boltzmann constant; T is the absolute temperature of the system; and λ_{B} is the Bjerrum length, defined as

$$\lambda_{\text{B}} = \frac{e^2}{4\pi\epsilon_0\epsilon_s k_{\text{B}} T} \quad (3)$$

where ϵ_0 is the permittivity of the free space, ϵ_s is the dielectric constant of the solvent, and e is the unit charge. The Bjerrum length is the separation distance between two unit charges at

which the electrostatic potential in the solution is equal to the thermal energy $k_{\text{B}} T$. It is set to 3σ in this study.

The bonded interactions between monomers in the dendrimers are modeled by the finitely extensible nonlinear elastic (FENE) potential function^{82,84}

$$U_{\text{FENE}}(r) = \begin{cases} -\frac{k}{2} R_0^2 \ln \left(1 - \frac{r^2}{R_0^2} \right) & r < R_0 \\ \infty & r \geq R_0 \end{cases} \quad (4)$$

where k is the bond force constant and R_0 is the maximum extension permitted for the bond. We set $k = 30(\epsilon/\sigma^2)$ and $R_0 = 1.5\sigma$ for the simulations.

We have performed Langevin dynamics simulations^{82,85–87} on the G3, G4, G5, G6, and G7 dendrimer systems by making use of the LAMMPS simulator.⁸⁸ The motion of each particle i is dictated by a total force \mathbf{F}_i^{T} acting on the particle, which consists of the forces arising from the interactions, a solvent friction, a random force, and the external electric field

$$m\ddot{\mathbf{r}}_i = \mathbf{F}_i^{\text{T}} = \mathbf{F}_i^{\text{I}} + \mathbf{F}_i^{\text{F}} + \mathbf{F}_i^{\text{R}} + \mathbf{F}_i^{\text{E}} \quad (5)$$

where m is the mass of the particle. The interaction force \mathbf{F}_i^{I} includes the LJ, Coulomb, and FENE interactions described above. The frictional force \mathbf{F}_i^{F} is modeled by $\mathbf{F}_i^{\text{F}} = -\xi_0 \mathbf{v}_i$, where \mathbf{v}_i is the velocity of the particle and ξ_0 is the friction coefficient. The random force \mathbf{F}_i^{R} originates from the random collisions with the solvent molecules, and the magnitude of the force satisfies the fluctuation–dissipation theorem:

$$\begin{aligned} \langle \mathbf{F}_i^{\text{R}}(t) \rangle &= 0 \\ \langle \mathbf{F}_i^{\text{R}}(t) \cdot \mathbf{F}_j^{\text{R}}(t') \rangle &= 6k_{\text{B}} T \xi_0 \delta_{ij} \delta(t - t') \end{aligned} \quad (6)$$

We assumed that all the particles have identical mass m and size σ and set the friction coefficient to $\xi_0 = 25m\tau^{-1}$, where $\tau = (m\sigma^2/\epsilon)^{1/2}$ defines the time unit of simulation. A Gaussian random variable of variance $2k_{\text{B}} T \xi_0$ was assigned to each component of \mathbf{F}_i^{R} at each simulation time step. This assignment controls the system temperature according to the fluctuation–dissipation theorem and is called the Langevin thermostat.⁸⁷ Here we set $k_{\text{B}} T = 1.2\epsilon$. The force exerted on particle i by the electric field applied in the z -direction is $\mathbf{F}_i^{\text{E}} = Z_i e \mathbf{E}_z$. We varied the strength of field from 0.0 to $7.8\epsilon e^{-1}\sigma^{-1}$.⁸⁹ When \mathbf{F}_i^{E} is in balance with \mathbf{F}_i^{F} , the system reaches a steady state and the charged particles drift at constant speeds in the solution. The drifting velocities persist under the Langevin thermostat and thus additionally increase the kinetic energy. Consequently, the system temperature increases. We have verified that the temperature increase is smaller than 3% of the setup temperature for the five systems studied. Therefore, the temperature is well controlled by the Langevin thermostat. Detailed information can be found in the Supporting Information (Figure S1).

In each of the G3, G4, G5, G6, and G7 cases, a single charged dendrimer is placed in a cubic simulation box of dimension 100σ ⁹⁰ with periodic boundary conditions.^{85,86} The Coulomb interactions were calculated using the particle–particle particle–mesh (PPPM) method.⁹¹ The root-mean-square force error in the PPPM calculation was set to 10^{-3} . The equation of motion was solved by the velocity-Verlet algorithm.^{82,85,86} The integration time step used for the generation of the trajectories equals $\Delta t = 0.005\tau$. The compositions of the five dendrimer systems are given in

Table 1. In order to understand the persistence of electrostatic effects in the electrolyte solutions, we have also provided the

Table 1. Composition of the Five Dendrimer Systems and the Debye Length of the Solutions

	G3	G4	G5	G6	G7
inner monomers	30	62	126	254	510
surface monomers	32	64	128	256	512
counterions	32	64	128	256	512
salt cations	11	22	43	86	171
salt anions	33	66	129	258	513
total no of particles	138	278	554	1110	2218
Debye length (σ)	12.72	8.99	6.42	4.54	3.22

Debye screening length λ_D in the table for reference. The Debye length was calculated by the formula $\lambda_D = 1/(8\pi l_B)^{1/2}$, where $I = (1/2)\sum_k c_k Z_k^2$ is the ionic strength of solution, c_k is the concentration, and Z_k is the valence of the ionic species k , including the counterions dissociated from the dendrimers, the salt cations, and the salt anions.

In each case, we analyze the trajectories of the system over 10^7 time steps after reaching a steady state to calculate the eigenvalues of the radius of gyration tensor, shape factors, distortion factor, and electrophoretic mobility of the dendrimer molecule along with radial density distribution and pair distribution functions of the monomers and ions. It is to be noted that, in the Langevin dynamics simulations, hydrodynamic interactions are not taken into account. It has been shown that the hydrodynamic effect plays an important role in the study of electrophoretic properties of charged systems.^{68–73} However, large computing resources and efforts are demanded if this effect is included in the simulations. For a first-step study here, we decided to neglect the hydrodynamic interactions to save simulation time, so that an overall picture of the dendrimer systems in electric fields can be captured.

In order to shorten the notation, physical quantities in the subsequent sections will be reported in terms of the (σ, ϵ, m, e) unit system.

3. RESULTS AND DISCUSSION

3.1. Radius of Gyration Tensor, Shape Factors, Orientation of Dendrimers, and Critical Field Strength.

The shape of a dendrimer molecule can be conveniently analyzed in terms of the radius of gyration tensor,⁹² which is defined as

$$T_{\alpha\beta} = \frac{1}{N} \sum_{i=1}^N (r_{\alpha,i} - r_{\alpha,\text{COM}})(r_{\beta,i} - r_{\beta,\text{COM}}) \quad (7)$$

with $\alpha, \beta \equiv x, y, z$. Here, $r_{\alpha,i}$ are the α th coordinates of the i th monomer and $r_{\alpha,\text{COM}}$ are the α th coordinates of the center of mass (COM) of the dendrimer.

Diagonalization of the 3×3 $[T_{\alpha\beta}]$ matrix yields the three eigenvalues λ_1, λ_2 , and λ_3 . We assume that $\lambda_1 \geq \lambda_2 \geq \lambda_3$. $(\lambda_1)^{1/2}$, $(\lambda_2)^{1/2}$, and $(\lambda_3)^{1/2}$ represent the three principal axes of an ellipsoidal structure formed by the dendrimer. Two shape factors are calculated: asphericity A and degree of prolateness P .⁷⁹ The asphericity A measures the deformation of a dendrimer from the spherical geometry and is defined by

$$A = \frac{(\lambda_1 - \lambda_2)^2 + (\lambda_2 - \lambda_3)^2 + (\lambda_3 - \lambda_1)^2}{2(\lambda_1 + \lambda_2 + \lambda_3)^2} \quad (8)$$

The value of A is 0 for a spherical structure and 1 for a rodlike structure. The degree of prolateness P estimates the type of ellipsoid that describes the distortion of a dendrimer caused by the electric field. It is defined as

$$P = \frac{(\lambda_1 - \bar{\lambda})(\lambda_2 - \bar{\lambda})(\lambda_3 - \bar{\lambda})}{\bar{\lambda}^3} \quad (9)$$

where $\bar{\lambda} = (1/3)(\lambda_1 + \lambda_2 + \lambda_3)$. A prolate ellipsoid is represented by values in the range $0 < P < 2$ and an oblate ellipsoid by $-0.25 < P < 0$.

In Figure 2, we present the individual eigenvalues λ_1, λ_2 , and λ_3 and the square of the radius of gyration R_g^2 of the G3, G4,

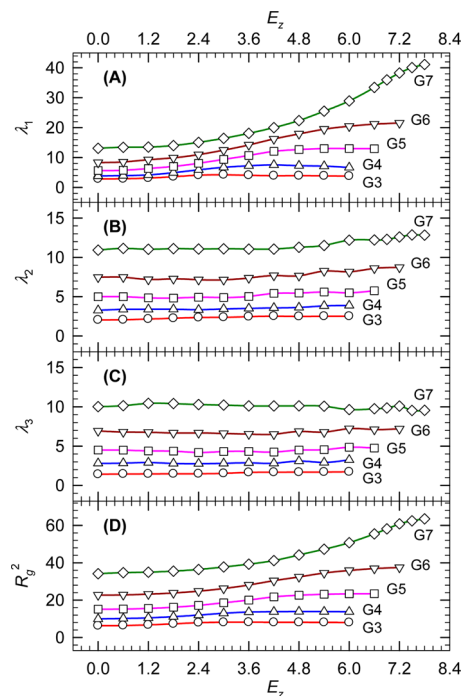


Figure 2. Mean eigenvalues λ_1, λ_2 , and λ_3 (sorted as $\lambda_1 > \lambda_2 > \lambda_3$) and the square of the radius of gyration R_g^2 of the G3, G4, G5, G6, and G7 dendrimers vs applied field strength E_z .

G5, G6, and G7 dendrimers as a function of E_z . R_g^2 is calculated by summing the three eigenvalues, $(\lambda_1 + \lambda_2 + \lambda_3)$.^{79,93}

We observe that λ_1 exhibits a sigmoidal increase with E_z , while λ_2 and λ_3 are essentially unaffected by the electric field. This is because the surface monomers (each with charge $-e$), together with the condensed cations, are polarized in the presence of the electric field. The polarization elongates the dendrimers along the field direction (i.e., the z -direction) and leaves the transverse directions (i.e., the x - and y -directions) unaffected. Therefore, the squared radius of gyration displays a behavior similar to that of λ_1 as a function of E_z . The sigmoid-like curve indicates a structural transition from a structure in weak electric fields to one in strong electric fields. The transition occurs at the critical fields $E_{z,\text{crit}} \approx 1.9, 2.3, 3.7, 4.2$, and 5.7 for the G3, G4, G5, G6, and G7 dendrimers, respectively, where $E_{z,\text{crit}}$ is estimated by the inflection point of the sigmoidal curve of fitting the R_g^2 data by the cubic spline method. There exist alternative potential definitions for this critical field. For example, the critical field is the field at which the polarization energy of a molecule is equal to the thermal energy,^{66,67} or where the onset of molecular distortion occurs.⁷⁶

The asphericity and the degree of prolateness curves as a function of E_z for the five dendrimer systems are shown in Figure 3. In weak electric fields, A and P are both zero and,

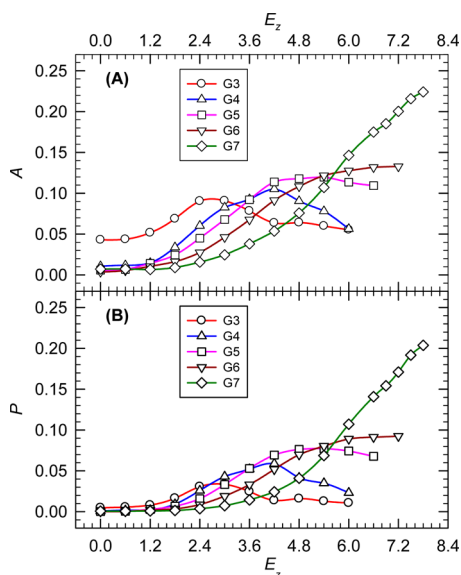


Figure 3. Asphericity A and degree of prolateness P as a function of the field strength E_z for the G3, G4, G5, G6, and G7 dendrimers.

thus, the dendrimers have a spherical structure, except for the G3 dendrimer because of the difficulty in forming a perfect sphere from such a small number of monomers (Table 1). As E_z increases, both A and P values increase and reach maxima at the same field strength and then decrease. The phenomena are understood as follows: The distortion of the dendrimer is assisted by the polarization of the dendrimer and the stripping-off of the condensed cations from the dendrimer surface. The polarization elongates the dendrimer molecule in the electric field, while the stripping-off tends to drive the dendrimer back to a near-spherical shape by reducing the polarization and also by increasing the net electrostatic repulsion inside the dendrimer. The interplay between these two effects results in the maxima seen in Figure 3. The detailed analysis about the variation of ion condensation with the electric field will be presented in the next section. We find that the higher the generation, the larger the maximum values of the asphericity and prolateness. This is because a large dendrimer allows a large distortion by the electric field. The inflection points obtained from the increasing portion of the A and P curves are practically consistent with the critical points obtained from the R_g^2 curve. These results are listed in Table 2 for comparison.

In addition to distorting the dendrimers' shape, the applied electric field can also alter the molecular orientation.^{66–77,94}

Table 2. Critical Field Strength $E_{z,\text{crit}}$ of the Five Dendrimer Systems Calculated from the λ_1 , R_g^2 , A , P , and μ Curves

property	critical field strength $E_{z,\text{crit}}$				
	G3	G4	G5	G6	G7
λ_1	1.89	2.26	3.61	4.20	5.70
R_g^2	1.97	2.35	3.74	4.27	5.64
A	1.91	2.25	3.66	4.09	5.75
P	1.93	2.32	3.80	4.16	5.86
μ	2.04	2.41	3.72	4.26	5.61

The orientation of a dendrimer is analyzed by calculating the order parameter as

$$S = \frac{1}{2}(3\langle \cos^2 \theta \rangle - 1) \quad (10)$$

where θ is the polar angle of the bond \vec{b}_{12} connecting monomer no. 1 and no. 2 in the dendrimer core (see Figure 1) with respect to the field direction. If the dendrimer is perfectly oriented along the field direction, then S is equal to 1, while $S = 0$ if it is randomly oriented.⁹⁵ Figure 4 presents the order parameters of the five dendrimer systems in the presence of electric fields.

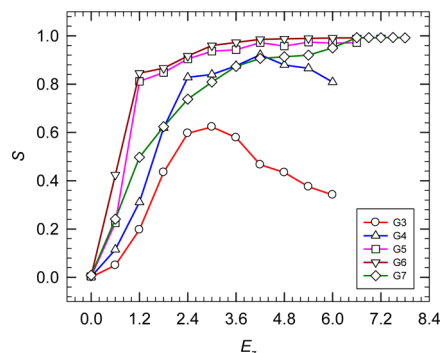


Figure 4. Order parameter S of the G3, G4, G5, G6, and G7 dendrimers as a function of electric field strength E_z .

In zero fields, the order parameter is zero, which shows a random orientation of the \vec{b}_{12} bond. As E_z increases, the value of S increases and tends to 1 for large enough dendrimers. Thus, \vec{b}_{12} aligns with the field direction. For small dendrimer systems, S displays a peak at $E_z = 3.0$ for the G3 system and 4.2 for the G4 system. The location of the peak corresponds to the peak of the asphericity A (Figure 3A) and degree of prolateness P (Figure 3B), which can be attributed to the occurrence of the maximum polarization. Beyond this position, the polarization effect decreases because of the stripping-off effect of the condensed ions. Consequently, the bond alignment reduces and, hence, S decreases. For large dendrimer systems (the G5 and G6 systems), a better alignment is observed, compared to the small systems. Since a substantial amount of salt cations are still condensed on the dendrimer in strong electric fields, the polarization energy is significantly larger than the thermal energy. The thermal agitation is not strong enough to destroy the order of the systems. As a result, the curve does not exhibit a peak.

The G7 system presents a slightly different case. In this system, the \vec{b}_{12} bond is immersed in a large number of the component monomers, which form a good spherical geometry. The uniqueness of the \vec{b}_{12} orientation is diluted. As a result, the polarization need not take place strictly along the bond direction and the increase in S is not as sharp as for the G5 and G6 systems.

3.2. Electrophoretic Mobility, Ion Condensation, Effective Charge, and Snapshots of the Dendrimers.

Electrophoretic mobility measures the migration of charged molecules through a solution under the influence of an applied electric field and is defined as the electrophoretic velocity v over the strength of the applied field,^{96,97} $\mu = v/E_z$. Figure 5 presents the electrophoretic mobility of the dendrimers as a function of the field strength.

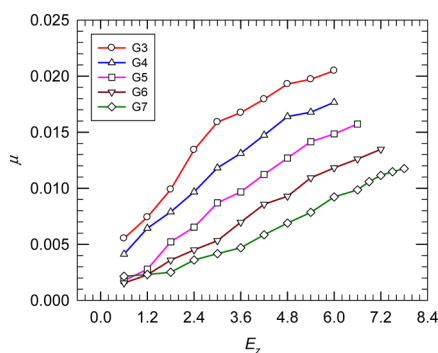


Figure 5. Electrophoretic mobility μ vs the field strength E_z for the G3, G4, G5, G6, and G7 dendrimers.

For a fixed field strength, the smaller the generation number, the higher the electrophoretic mobility. At a given generation, the mobility increases with the electric field. The inflection point of the curve occurs at a field strength consistent with the critical value obtained from the λ_1 , R_g^2 , A , and P curves, as shown in Table 2.

Theoretically, the electrophoretic mobility μ is equal to $|q_{\text{eff}}|/\xi_{\text{eff}}$, where $|q_{\text{eff}}|$ is the effective charge carried by a dendrimer molecule and ξ_{eff} is the effective friction coefficient. In our Langevin simulations, the hydrodynamic interactions are neglected and, thus, the system is described by Rouse dynamics. Consequently, ξ_{eff} is equal to $(N + N_c)\xi_0$, regardless of conformation, where N is the number of monomers in the dendrimer, N_c is the number of ions condensing on the dendrimer, and ξ_0 is the friction coefficient of a single monomer from the Langevin thermostat parameter. Even without electrohydrodynamics, the values of $|q_{\text{eff}}|$ and ξ_{eff} both depend on ion condensation. To understand this effect more precisely, we calculate the number of ions condensed on a dendrimer. An ion is said to be condensed if the shortest distance from the ion to any monomer of the dendrimer is smaller than the Bjerrum length λ_B . When this criterion is satisfied, the electrostatic binding energy between a counterion and a charged monomer is larger than the thermal energy $k_B T$ and the counterion is said to be bound to the dendrimer against thermal fluctuations. Similar criteria have been used to study mobility change of polyelectrolytes in electric fields.^{66,67,70–72,75–77} In our case, the condensed ions are mainly the trivalent salt cations. Figure 6A presents the variation of the ratio $N_{c,+3}/N_{+3}$ in electric fields of the number $N_{c,+3}$ of the condensed trivalent cations out of the total number N_{+3} of trivalent cations in the system.

Since the dendrimer surface is highly charged, most of the trivalent salt cations condense on the surface due to strong electrostatic interactions. The ratio $N_{c,+3}/N_{+3}$ is close to 1 in zero fields. Increasing E_z decreases the ratio. The ratio decreases more rapidly for the dendrimers with smaller generation number. Owing to the stripping-off effect of the condensed ions in the strong fields, the dendrimer becomes less neutralized. This causes a net decrease in ξ_{eff} and an increase in $|q_{\text{eff}}|$, which causes the electrophoretic mobility $\mu = |q_{\text{eff}}|/\xi_{\text{eff}}$ to increase with the field strength, as shown in Figure 5. Also, at a given field strength, the condensation ratio is smaller for the system with smaller generation number, leading to a larger mobility, in agreement with Figure 5. Grass and Holm have proposed a precise estimator for ion condensation onto polyelectrolytes in Langevin dynamics simulations.⁷¹ Given

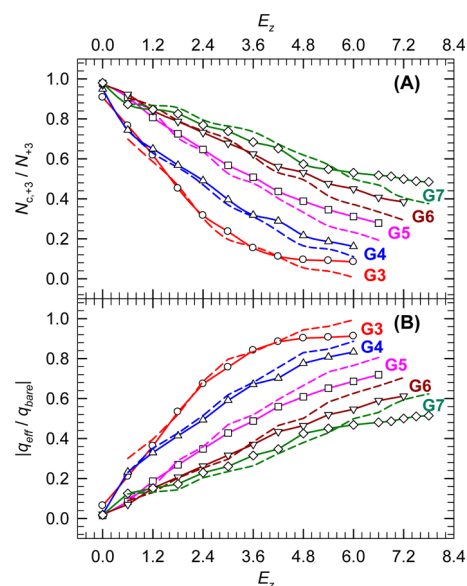


Figure 6. (A) Fraction $N_{c,+3}/N_{+3}$ of trivalent salt cations condensed on the dendrimer surface and (B) ratio $|q_{\text{eff}}|/|q_{\text{bare}}|$ of effective charge to bare charge of the dendrimer as a function of the field strength E_z for the G3, G4, G5, G6, and G7 dendrimers. Symbol and solid curves represent the values calculated directly from the dendrimer–ion distance smaller than the Bjerrum length. Dashed curves are the results calculated from the electrophoretic mobility values shown in Figure 5.

the measured value of the electrophoretic mobility μ , the number of the condensed trivalent cations $N_{c,+3}$ can be calculated from the equation

$$\mu = |-eN_s + 3eN_{c,+3}|/\xi_0(N + N_{c,+3}) \quad (11)$$

where N_s is the number of surface monomers, which is related to the total number of monomers by $N_s = (N + 2)/2$. Reorganization of eq 11 yields

$$N_{c,+3} = N \cdot \frac{\left(\frac{1}{2} + \frac{1}{N} - \frac{\xi_0 \mu}{e}\right)}{\left(3 + \frac{\xi_0 \mu}{e}\right)} \quad (12)$$

We plot $N_{c,+3}/N_{+3}$ in Figure 6A (dashed curves) using this estimator. The estimator gives a consistent result with the previous one, except in the strong fields considered. The distance-criterion method somewhat overestimates the number of condensed cations in the strong fields but, in general, is a good estimator.

The applied electric field polarizes the dendrimer-condensed ion systems by shifting the surface monomers toward the $-z$ -direction and the condensed trivalent cations toward the $+z$ -direction and, hence, elongates the conformation of the dendrimers. The larger the separation between surface monomers and cations, the larger the polarization. However, the electric field also strips off the condensed ions from the dendrimer, which effectively reduces the polarization. The two effects compete with each other and result in the maximum polarization, manifested in the peaks shown in the A and P curves in parts A and B of Figure 3, respectively. When dendrimers are subject to even stronger electric fields, so many of the condensed cations are stripped off that the effective charge $|q_{\text{eff}}|$ begins to increase significantly. The Coulomb repulsion inside the dendrimer portion thus increases, which leads to a less-elongated structure and hence a decrease of A

and P . The ratio of the effective charge to the bare charge of the dendrimer, $|q_{\text{eff}}/q_{\text{bare}}| = 1 - (3N_{\text{c},+3}/N_{\text{s}})$, is plotted in Figure 6B as a function of E_z . We find that the peaks of the A and P curves (Figure 3) for the G3, G4, G5, and G6 systems (at $E_z = 2.4, 4.2, 5.6$, and 7.0 , respectively) all occur at the moment when the effective charge ratio is approximately 0.7. This demonstrates the importance of ion condensation behavior in electric fields on the shape distortion and maximum polarization of dendrimers. Noticeably, it is easier to strip-off the condensed ions from a smaller dendrimer system. This trend is different from linear polyelectrolyte systems, in which the stripping-off of the condensed counterions is more difficult in a shorter chain, compared to a longer chain.^{66,67,75,76}

For linear polyelectrolytes, a phenomenon called the “free-draining effect” is well-known. The electrophoretic mobility becomes length-independent when the chain length is longer than the Debye length.^{68,70,98,99} The effective friction of the polymer chain scales linearly with the monomer number of chain, and not with the radius of gyration, showing a Rouse-like behavior. Therefore, to separate polyelectrolytes in free solutions in electric fields, according to the chain length, is impossible. It is generally attributed to the correlated motion of the ions surrounding the chain monomers, which effectively cancels the hydrodynamic effect.^{68–73} In the case of charged dendrimers, such a molecular-size-independent phenomenon has not been observed in experiments.⁶⁵ In our study, the computed electrophoretic mobility does show a dependence on the generation number (Figure 5). Thus, one can separate charged dendrimers of different generations in free solutions using conventional electrophoretic techniques. Smaller dendrimers exhibit larger mobilities (due to larger effective charge-to-friction ratios), which shorten the migration time. Of course, a systematic study is necessitated to incorporate the hydrodynamic interactions in simulations in the future, which would clarify the impact of the long-range hydrodynamics on the underlying mechanism of dendrimer migration in electric fields.

Figure 7 shows simulation snapshots of the G3 and G7 dendrimers. The conformation of dendrimer exhibits a spherical structure in the zero field, and almost all the trivalent cations condense onto the dendrimer. In a strong electric field $E_z = 6$, the dendrimer is elongated along the z -direction and a substantial number of the $+3$ ions are forced to detach from the dendrimer surface.

3.3. Density Distributions and Pair Correlation Functions. The conformation of a macromolecule depends very much on the distribution of its constituents in the three-dimensional space and its interactions with the surroundings. Therefore, we study the density distributions and the pair correlation functions for the G5 dendrimer system. The G5 system is particularly relevant because the PAMAM-G5 is often used as an encapsulator for drug delivery.^{13–15,100,101}

We have shown how the charged constituents are polarized in an asymmetric way in electric fields: the surface monomers of dendrimer are shifted toward the $-z$ -direction while the condensed salt cations toward the $+z$ -direction. To highlight this effect, we calculate the mean radial density distributions of the charged constituents in the upper and lower hemispherical spaces separately. The upper (lower) space is defined to be the space region with the z -coordinate lying above (below) the dendrimer center. The two distributions for the surface monomers are calculated as follows:

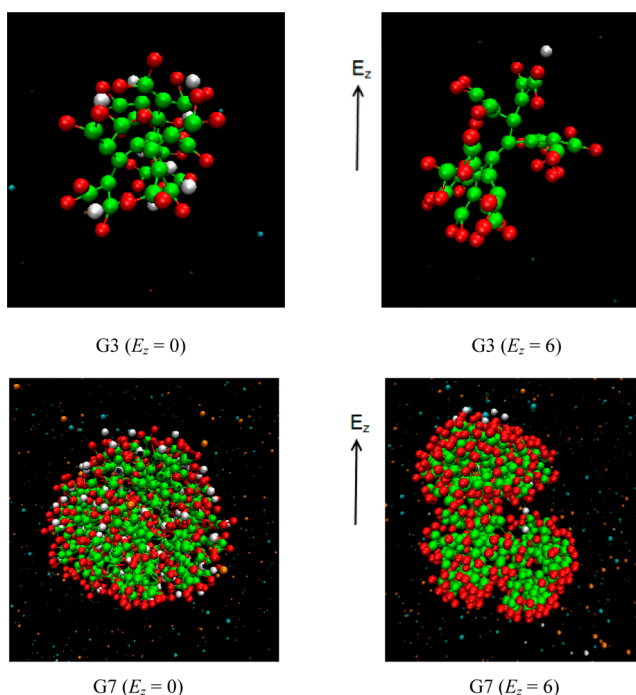


Figure 7. Snapshots of the G3 and G7 systems at $E_z = 0$ and 6. The inner monomers, the surface monomers, the dendrimer counterions, the trivalent salt cations, and the salt anions are represented by the green, red, orange, white, and light blue beads, respectively.

$$\rho_{\text{sm}}^{(\text{u})}(r) = \frac{N_{\text{sm}}^{(\text{u})}(r)}{2\pi r^2 dr} \quad (13a)$$

$$\rho_{\text{sm}}^{(\text{l})}(r) = \frac{N_{\text{sm}}^{(\text{l})}(r)}{2\pi r^2 dr} \quad (13b)$$

where $N_{\text{sm}}^{(\text{u})}(r)$ and $N_{\text{sm}}^{(\text{l})}(r)$ are the numbers of the surface monomers located in the upper and lower hemispherical shell with a distance $(r, r + dr)$ from the center of the dendrimer, respectively. Figure 8 presents the results of the calculations. For comparison, $\rho_{\text{sm}}^{(\text{l})}(r)$ is plotted in the left panel of the figure and $\rho_{\text{sm}}^{(\text{u})}(r)$ in the right panel.

In the zero field, $\rho_{\text{sm}}^{(\text{l})}(r)$ is mirror-symmetric to $\rho_{\text{sm}}^{(\text{u})}(r)$. The two distributions exhibit a two-peak profile, which shows that a

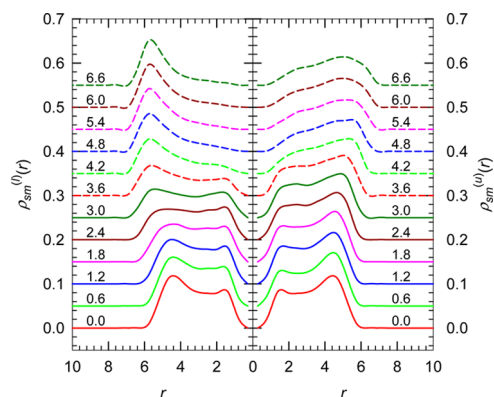


Figure 8. Mean radial density distributions, $\rho_{\text{sm}}^{(\text{l})}(r)$ and $\rho_{\text{sm}}^{(\text{u})}(r)$, in various electric field strengths for the G5 system. Each curve has been shifted vertically by 0.05 for clarity. The numbers adjacent to the curves are the strength of electric fields E_z .

portion of the surface monomers are folded inward and located closer to the dendrimer center, while the rest are folded outward and remain in the outer shell. The inward-folding peak (at smaller r) is formed because the trivalent salt cations can penetrate into the interior of the dendrimer where a large vacant space exists because of the branched structure of the dendrimer.^{102,103} Consequently, some of the surface monomers are attracted by the trivalent salt cations into the interior of the dendrimer. When an electric field is applied, the two density distributions gradually shift outward and an asymmetric evolution between the profiles is revealed. When the field strength is increased above the critical field $E_{z,\text{crit}} \approx 3.6$ (obtained in section 3.2), the distributions transform from a two-peak profile to a one-peak profile. In such strong external fields, the surface monomers reside mainly on the outer shell and are more concentrated in the lower hemisphere (with a sharper peak in $\rho_{\text{sm}}^{(l)}(r)$) than in the upper one.

The polarization takes place only when cations condense on the dendrimer. In order to understand the interplay between the trivalent salt cations and the surface monomers, we study the mean radial density distributions of the cations, $\rho_{+3}^{(l)}(r)$ and $\rho_{+3}^{(u)}(r)$, in the two hemispheres. The calculation method is identical to the one for the surface monomers except that $N_{\text{sm}}^{(u)}(r)$ and $N_{\text{sm}}^{(l)}(r)$ are replaced by the number of the +3 cations in the upper and lower hemispherical shells, $N_{+3}^{(u)}(r)$ and $N_{+3}^{(l)}(r)$, respectively. The results are presented in Figure 9.

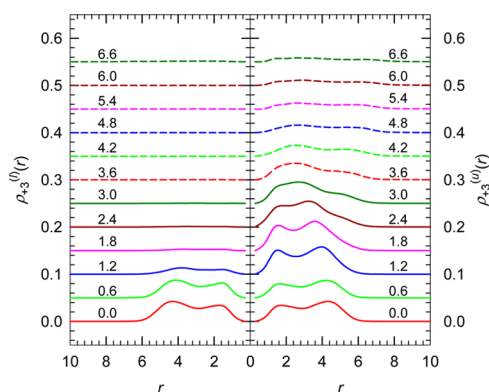


Figure 9. Mean radial density distributions, $\rho_{+3}^{(l)}(r)$ and $\rho_{+3}^{(u)}(r)$, in various electric field strengths for the G5 system. Each curve has been shifted vertically by 0.05 for clarity. The numbers adjacent to the curves are the strength of electric fields E_z .

We observe that both $\rho_{+3}^{(l)}(r)$ and $\rho_{+3}^{(u)}(r)$ display a two-peak profile, mirror-symmetric to each other in the zero field, as we previously observed in the $\rho_{\text{sm}}^{(l)}(r)$ and $\rho_{\text{sm}}^{(u)}(r)$ distributions. The magnitude of the density is about one-third of that of the surface monomers, showing that the surface monomers are essentially neutralized by the condensed trivalent cations. When an external electric field is applied, the polarization displaces the charged particles, making the distribution asymmetric.

An interesting feature that emerges is that the +3 cations are forced to strip off from the lower hemisphere of the dendrimer first. A near-complete stripping occurs at about $E_z = 1.8$. Beyond this field strength, a gradual stripping in the upper hemisphere takes place and the two-peak profile then transforms to a single-peak profile around $E_z = 3.6$, followed by a further lowering of the peak value. By comparing Figure 9 to Figure 8, we can determine that the peak is located in the

interior of the upper hemisphere of the dendrimer due to the polarization in the strong electric fields.

To understand effective interaction between surface monomers and trivalent salt cations, we calculate the pair correlation functions between them

$$g_{\text{sm},+3}(r) = \left(\frac{V}{N_{\text{sm}}N_{+3}} \right) \cdot \left[\frac{N_{\text{sm},+3}(r)}{4\pi r^2 dr} \right] \quad (14)$$

where $N_{\text{sm},+3}(r)$ is the mean number of pairs between surface monomers and trivalent salt cations within the distance lying between $(r, r + dr)$, N_{sm} and N_{+3} are the number of surface monomers and trivalent salt cations in the system, respectively, and V is the volume of simulation box.

We observe from Figure 10 that the pair correlation function $g_{\text{sm},+3}(r)$ exhibits a strong peak at $r \approx 1.9\sigma$ in the no field case.

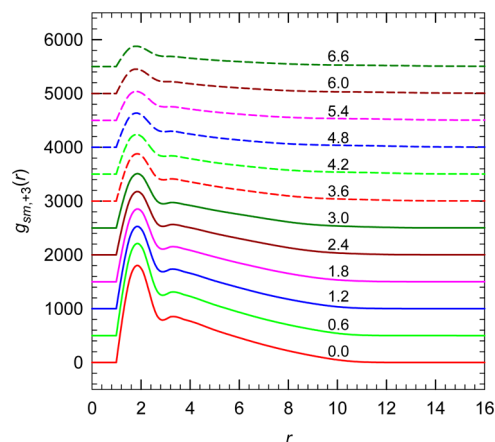


Figure 10. Pair correlation function between surface monomers and salt cations in the G5 system, in various electric field strengths. Successive curves have been shifted vertically by 500 for the sake of clarity. The numbers adjacent to the curves are the strength of electric fields E_z .

This is expected, as the surface monomers are mostly neutralized by the condensed trivalent salt cations and each trivalent cation seeks three surface monomers to obtain charge neutralization. The peak height gradually decreases with increasing electric field, which can be attributed to the stripping of the +3 cations from the dendrimer. The local density of the ions surrounding the surface monomers, and hence the pair correlation, decreases. Moreover, the range of the pair-correlation extends in strong electric fields, owing to the electric polarization increasing the separation distance between salt cations and the monomers.

3.4. Scaling Behavior and Master Curves. The structure of dendrimer molecules exhibits fractal resemblance with respect to the generation number and the total number of monomers. The first property to be studied is the critical field strength required to distort the dendrimers. Figure 11 presents the $E_{z,\text{crit}}$ obtained from λ_1 , R_g^2 , A , P , and μ , as a function of the number of monomers N .

In the log–log plot, the five sets of data exhibit a linear-dependence relationship, showing that the critical field requirement follows a scaling behavior. The linear regression line obtained by least-squares fitting of the data yields $E_{z,\text{crit}} \sim N^{0.39(6)}$. Therefore, it is more difficult to distort a dendrimer molecule of larger generation number. This positive scaling exponent is different from what is observed for the unfolding of

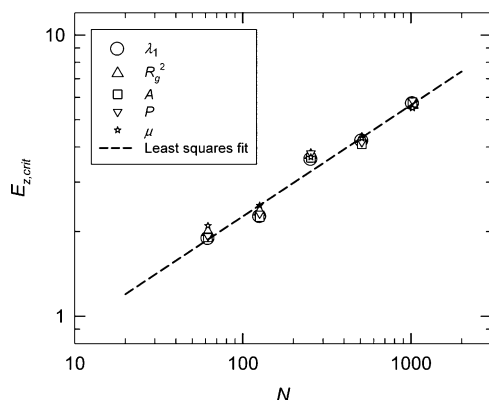


Figure 11. Critical field strength $E_{z,\text{crit}}$ obtained from λ_1 , R_g^2 , A , P , and μ as a function of the number of monomers N .

collapsed polyelectrolyte chains in electric fields, where the critical field scales with the number of monomers N with a negative exponent.^{66,67,75,76,94} It is easier to unfold longer polyelectrolytes than shorter but more arduous to distort dendrimers of larger generation number than smaller.

The values of λ_1 , R_g^2 , A , P , and μ at the critical field strength $E_{z,\text{crit}}$ also follow a scaling relation N^β . The exponents β are 0.72, 0.66, 0.27, 0.54, and -0.15 for λ_1 , R_g^2 , A , P , and μ , respectively (see the Supporting Information, Figure S3). By dividing the x - and y -axes by the scaling relation $N^{0.39(6)}$ and N^β , respectively, we observe in Figure 12 that the curves roughly overlap into single master curves, except the curves for the smallest G3 system. This result demonstrates a universal scaling behavior and suggests that the properties of dendrimers can be theoretically approached by the renormalization group method.^{21,104–106}

It has been a subject of study to understand how the size of a dendrimer (radius of gyration R_g) scales with the number of monomers N .^{8,19–44} Figure 13A presents our simulation results in the zero field. The least-squares fitting yields a scaling relation, $R_g \sim N^{0.29}$. The derived relation matches closely with that of Murat and Grest²⁴ and also with Sheng et al.⁸ However, there exists no unanimity about the value of the exponent, as pointed out by Klos and Sommer.³⁶ We notice that dendrimer size also follows an approximate scaling relation with respect to the generation number n . From these simulation results, the scaling law in zero field is $R_g \sim n^{1.04}$. We plot the results in Figure 13B for comparison.

4. CONCLUSIONS

We have investigated the behavior of surface charged dendrimers of generations G3, G4, G5, G6, and G7 in trivalent salt solutions under the action of DC electric fields. The size and shape of dendrimers have been studied by calculating the radius of gyration tensor. The square of the radius of gyration R_g^2 , the asphericity shape factor A , and the degree of prolateness P exhibited marked deviations beyond a critical field strength $E_{z,\text{crit}}$ derived from the strong polarization effect which distorts the dendrimers by elongation. The degree of distortion of these dendrimers is much smaller than for linear polyelectrolytes in electric fields. When the strength of the electric field is increased, condensed ions begin to strip off the dendrimers, which reduces the distortion. The orientation of dendrimer molecules showed an alignment of molecular orientation to the electric fields in the strong field intensity.

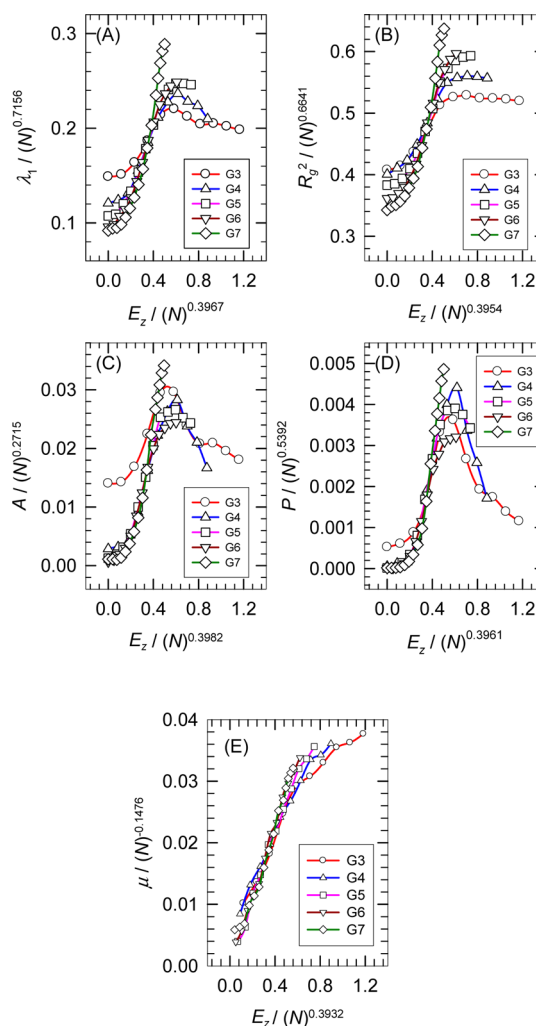


Figure 12. Master curves for the properties λ_1 , R_g^2 , A , P , and μ of the dendrimers. The abscissa is divided by $N^{0.39(6)}$, while the ordinate is divided by N^β . β is 0.72, 0.66, 0.27, 0.54, and -0.15 for λ_1 , R_g^2 , A , P , and μ , respectively.

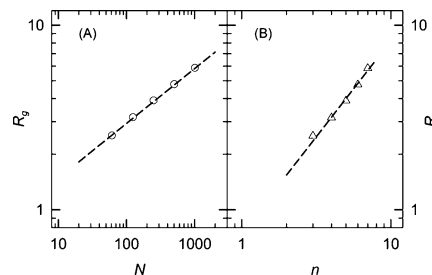


Figure 13. Zero field scaling laws for the radius of gyration of dendrimers with (A) the number of monomers N and (B) the generation number n . The dashed lines are the least-squares fits of the data.

The electrophoretic mobility increases with field strength and forms a sigmoidal curve for a given generation number. The higher the generation number, the smaller the mobility. The results are mainly dominated by the decrease in the number of condensed trivalent cations, which are stripped off by strong electric fields. This increases the effective charge of the dendrimer, leading to a rise in the mobility. The electrophoretic mobility can be better understood by incorporating long-range

hydrodynamic interactions in the dendrimer simulations. We are working on this aspect now, and the results will be published in the future.

To understand the charge polarization in the dendrimers, the radial densities of the surface monomers and of the salt cations were calculated in the upper and lower hemispherical spaces along the field direction. The densities transformed gradually from mirror-symmetric profiles to asymmetric ones, showing how the polarization proceeded with increasing the electric fields. The stripping-off of condensed ions from the dendrimer surface was especially apparent in the radial densities. This effect was also seen in the pair correlation function between the surface monomers and the salt cations, in which the intensity of the primary peak at $r \approx 1.9\sigma$ decreases as the electric field increases.

Finally, our simulations show that the critical field strength $E_{z,\text{crit}}$ required to deform the dendrimers scales with monomer number as $E_{z,\text{crit}} \sim N^{0.39(6)}$. The similarity of the curves for the properties λ_1 , R_g^2 , A , P , and μ as a function of field intensity E_z over many dendrimer generations further allowed us to collapse the family curves into single master curves by appropriate transformations. Such master curves show a surprising fractal resemblance in such dendrimer systems and suggest that a renormalization group approach to dendrimers in electric fields may be a fruitful venture. The results of this study may provide useful information for researchers to predict, analyze, and control dendrimers in drug delivery and many broad applications.

■ ASSOCIATED CONTENT

● Supporting Information

Details of the temperature control and total energy of the simulation systems along with a remark on the thermostat used. We have also elaborated the scaling laws for the quantities λ_1 , R_g^2 , A , P , and μ at the critical fields. This material is available free of charge via the Internet at <http://pubs.acs.org>.

■ AUTHOR INFORMATION

Corresponding Author

*E-mail: pyhsiao@ess.nthu.edu.tw.

Notes

The authors declare no competing financial interest.

■ ACKNOWLEDGMENTS

The authors thank Tyler N. Shendruk for reading the manuscript and the comments. This material is based upon work supported by the National Science Council (NSC), Taiwan, under the Grant Nos. NSC 100-2112-M-007-002-MY3, NSC 102-2811-M-007-001, and NSC 103-2811-M-007-002.

■ REFERENCES

- (1) Westermeier, R. *Electrophoresis in Practice*, 4th ed.; Wiley-VCH: Weinheim, Germany, 2005.
- (2) Robinson, J. R.; Lee, V. H., Eds. *Controlled Drug Delivery: Fundamentals and Applications*, 2nd ed.; Marcel Dekker: New York, 1987.
- (3) Chang, D. C. *Guide to Electroporation and Electrofusion*; Academic Press: New York, 1992.
- (4) DeGuzman, V. S.; Lee, C. C.; Deamer, D. W.; Vercoutere, W. A. Sequence-dependent gating of an ion channel by DNA hairpin molecules. *Nucleic Acids Res.* **2006**, *34*, 6425–6437.
- (5) Hadjichristidis, N.; Hirao, A.; Tezuka, Y.; Prez, F. D., Eds. *Complex Macromolecular Architectures: Synthesis, Characterization and Self-assembly*; John Wiley & Sons: Singapore, 2011.
- (6) Huißmann, S.; Likos, C. N.; Blaak, R. Conformations of high-generation dendritic polyelectrolytes. *J. Mater. Chem.* **2010**, *20*, 10486–10494.
- (7) Blaak, R.; Lehmann, S.; Likos, C. N. Charge-induced conformational changes of dendrimers. *Macromolecules* **2008**, *41*, 4452–4458.
- (8) Sheng, Y. J.; Jiang, S.; Tsao, H. K. Radial size of a starburst dendrimer in solvents of varying quality. *Macromolecules* **2002**, *35*, 7865–7868.
- (9) Hirao, A.; Sugiyama, K.; Yokoyama, H. Precise synthesis and surface structures of architectural per-and semifluorinated polymers with well-defined structures. *Prog. Polym. Sci.* **2007**, *32*, 1393–1438.
- (10) Caminade, A. M.; Turin, C. O.; Laurent, R.; Ouali, A.; Nicot, B. D. *Dendrimers: Towards Catalytic, Material and Biomedical Uses*; John Wiley & Sons: Chichester, U.K., 2011.
- (11) Scott, R. W. J.; Wilson, O. M.; Crooks, R. M. Synthesis, characterization, and applications of dendrimer-encapsulated nanoparticles. *J. Phys. Chem. B* **2005**, *109*, 692–704.
- (12) Cheng, Y., Ed. *Dendrimer-based Drug Delivery Systems: From Theory to Practice*; John Wiley & Sons: Hoboken, NJ, 2012.
- (13) Patri, A. K.; Kukowska-Latallo, J. F.; Baker, J. R., Jr Targeted drug delivery with dendrimers: comparison of the release kinetics of covalently conjugated drug and non-covalent drug inclusion complex. *Adv. Drug Delivery Rev.* **2005**, *57*, 2203–2214.
- (14) Patri, A. K.; Majoros, I. J.; Baker, J. R., Jr Dendritic polymer macromolecular carriers for drug delivery. *Curr. Opin. Chem. Biol.* **2002**, *6*, 466–471.
- (15) Tomalia, D. A.; Reyna, L. A.; Svenson, S. Dendrimers as multi-purpose nanodevices for oncology drug delivery and diagnostic imaging. *Biochem. Soc. Trans.* **2007**, *35*, 61–67.
- (16) Kukowska-Latallo, J. F.; Bielinska, A. U.; Johnson, J.; Spindler, R.; Tomalia, D. A.; Baker, J. R. Efficient transfer of genetic material into mammalian cells using Starburst polyamidoamine dendrimers. *Proc. Natl. Acad. Sci. U.S.A.* **1996**, *93*, 4897–4902.
- (17) Bosman, A. W.; Janssen, H. M.; Meijer, E. W. About dendrimers: structure, physical properties, and applications. *Chem. Rev.* **1999**, *99*, 1665–1688.
- (18) Medina, S. H.; El-Sayed, M. E. Dendrimers as carriers for delivery of chemotherapeutic agents. *Chem. Rev.* **2009**, *109*, 3141–3157.
- (19) Tian, W.; Ma, Y. Theoretical and computational studies of dendrimers as delivery vectors. *Chem. Soc. Rev.* **2013**, *42*, 705–727.
- (20) de Gennes, P. G.; Hervet, H. Statistics of starburst polymers. *J. Phys., Lett.* **1983**, *44*, 351–360.
- (21) Boris, D.; Rubinstein, M. A self-consistent mean field model of a starburst dendrimer: dense core vs dense shell. *Macromolecules* **1996**, *29*, 7251–7260.
- (22) Giupponi, G.; Buzza, D. M. A. A Monte Carlo study of amphiphilic dendrimers: Spontaneous asymmetry and dendron separation. *J. Chem. Phys.* **2005**, *122*, 194903.
- (23) Lescanec, R. L.; Muthukumar, M. Configurational characteristics and scaling behavior of starburst molecules: a computational study. *Macromolecules* **1990**, *23*, 2280–2288.
- (24) Murat, M.; Grest, G. S. Molecular dynamics study of dendrimer molecules in solvents of varying quality. *Macromolecules* **1996**, *29*, 1278–1285.
- (25) Chen, Z. Y.; Cui, S. M. Monte Carlo simulations of star-burst dendrimers. *Macromolecules* **1996**, *29*, 7943–7952.
- (26) Giupponi, G.; Buzza, D. M. A. A Monte Carlo simulation scheme for nonideal dendrimers satisfying detailed balance. *Macromolecules* **2002**, *35*, 9799–9812.
- (27) Timoshenko, E. G.; Kuznestov, Y. A.; Connolly, R. Conformations of dendrimers in dilute solution. *J. Chem. Phys.* **2002**, *117*, 9050–9062.
- (28) Götze, I. O.; Likos, C. N. Conformations of flexible dendrimers: a simulation study. *Macromolecules* **2003**, *36*, 8189–8197.

- (29) Rathgeber, S.; Pakula, T.; Urban, V. Structure of star-burst dendrimers: A comparison between small angle x-ray scattering and computer simulation results. *J. Chem. Phys.* **2004**, *121*, 3840–3853.
- (30) (a) Lyulin, S. V.; Evers, L. J.; van der Schoot, P.; Darinskii, A. A.; Lyulin, A. V.; Michels, M. A. J. Effect of solvent quality and electrostatic interactions on size and structure of dendrimers. Brownian dynamics simulation and mean-field theory. *Macromolecules* **2004**, *37*, 3049–3063. (b) Lyulin, S. V.; Darinskii, A. A.; Lyulin, A. V.; Michels, M. A. J. Computer simulation of the dynamics of neutral and charged dendrimers. *Macromolecules* **2004**, *37*, 4676–4685.
- (31) Rissanou, A. N.; Economou, I. G.; Panagiotopoulos, A. Z. Monte Carlo simulation of the phase behavior of model dendrimers. *Macromolecules* **2006**, *39*, 6298–6305.
- (32) Timoshenko, E. G.; Kuznestov, Y. A.; Simonov, G. E. Conformations of isolated ampholytic dendrimers in solutions. *Phys. A (Amsterdam, Neth.)* **2007**, *379*, 23–31.
- (33) Klos, J. S.; Sommer, J. U. Properties of dendrimers with flexible spacer-chains: a Monte Carlo study. *Macromolecules* **2009**, *42*, 4878–4886.
- (34) Klos, J. S.; Sommer, J. U. Simulations of terminally charged dendrimers with flexible spacer chains and explicit counterions. *Macromolecules* **2010**, *43*, 4418–4427.
- (35) Klos, J. S.; Sommer, J. U. Simulations of dendrimers with flexible spacer chains and explicit counterions under low and neutral pH conditions. *Macromolecules* **2010**, *43*, 10659–10667.
- (36) Klos, J. S.; Sommer, J. U. Simulations of Neutral and Charged Dendrimers in Solvents of Varying Quality. *Macromolecules* **2013**, *46*, 3107–3117.
- (37) Bosko, J. T.; Prakash, J. R. Effect of molecular topology on the transport properties of dendrimers in dilute solution at theta temperature: A Brownian dynamics study. *J. Chem. Phys.* **2008**, *128*, 034902.
- (38) Scherrenberg, R.; Coussens, B.; van Vliet, P.; Edouard, G.; Brackman, J.; de Brabander, E.; Mortensen, K. The molecular characteristics of poly (propyleneimine) dendrimers as studied with small-angle neutron scattering, viscosimetry, and molecular dynamics. *Macromolecules* **1998**, *31*, 456–461.
- (39) Cavallo, L.; Fraternali, F. A Molecular Dynamics Study of the First Five Generations of Poly (Propylene Imine) Dendrimers Modified with N-tBoc-L-Phenylalanine. *Chem. Eur. J.* **1998**, *4*, 927–934.
- (40) Zacharopoulos, N.; Economou, I. G. Morphology and organization of poly (propylene imine) dendrimers in the melt from molecular dynamics simulation. *Macromolecules* **2002**, *35*, 1814–1821.
- (41) Maiti, P. K.; Cagin, T.; Wang, G.; Goddard, W. A. Structure of PAMAM dendrimers: Generations 1 through 11. *Macromolecules* **2004**, *37*, 6236–6254.
- (42) Maiti, P. K.; Cagin, T.; Lin, S. T.; Goddard, W. A. Effect of solvent and pH on the structure of PAMAM dendrimers. *Macromolecules* **2005**, *38*, 979–991.
- (43) Tian, W.; Ma, Y. Molecular dynamics simulations of a charged dendrimer in multivalent salt solution. *J. Phys. Chem. B* **2009**, *113*, 13161–13170.
- (44) Tian, W.; Ma, Y. Effects of valences of salt ions at various concentrations on charged dendrimers. *Soft Matter* **2010**, *6*, 1308–1316.
- (45) Stechemesser, S.; Eimer, W. Solvent-dependent swelling of poly (amido amine) starburst dendrimers. *Macromolecules* **1997**, *30*, 2204–2206.
- (46) Nisato, G.; Ivkov, R.; Amis, E. J. Size invariance of polyelectrolyte dendrimers. *Macromolecules* **2000**, *33*, 4172–4176.
- (47) Lombardo, D. Liquid-like ordering of negatively charged poly (amidoamine) (PAMAM) dendrimers in solution. *Langmuir* **2009**, *25*, 3271–3275.
- (48) Uppuluri, S.; Keinath, S. E.; Tomalia, D. A.; Dvornic, P. R. Rheology of dendrimers. I. Newtonian flow behavior of medium and highly concentrated solutions of polyamidoamine (PAMAM) dendrimers in ethylenediamine (EDA) solvent. *Macromolecules* **1998**, *31*, 4498–4510.
- (49) Haba, Y.; Harada, A.; Takagishi, T.; Kono, K. Rendering poly (amidoamine) or poly (propyleneimine) dendrimers temperature sensitive. *J. Am. Chem. Soc.* **2004**, *126*, 12760–12761.
- (50) Chen, W.; Tomalia, D. A.; Thomas, J. L. Unusual pH-dependent polarity changes in PAMAM dendrimers: evidence for pH-responsive conformational changes. *Macromolecules* **2000**, *33*, 9169–9172.
- (51) Cakara, D.; Kleimann, J.; Borkovec, M. Microscopic protonation equilibria of poly (amidoamine) dendrimers from macroscopic titrations. *Macromolecules* **2003**, *36*, 4201–4207.
- (52) Terao, T.; Nakayama, T. Molecular dynamics study of dendrimers: Structure and effective interaction. *Macromolecules* **2004**, *37*, 4686–4694.
- (53) Gurtovenko, A. A.; Lyulin, S. V.; Karttunen, M.; Vattulainen, I. Molecular dynamics study of charged dendrimers in salt-free solution: Effect of counterions. *J. Chem. Phys.* **2006**, *124*, 094904.
- (54) Giupponi, G.; Buzza, D. M. A.; Adolf, D. B. Are polyelectrolyte dendrimers stimuli responsive? *Macromolecules* **2007**, *40*, S959–S965.
- (55) Seyrek, E.; Dubin, P. L.; Newkome, G. R. Effect of electric field on the mobility of carboxyl-terminated dendrimers. *J. Phys. Chem. B* **2004**, *108*, 10168–10171.
- (56) Hong, S.; Bielinska, A. U.; Mecke, A.; Keszler, B.; Beals, J. L.; Shi, X.; Banaszak Holl, M. M. Interaction of poly (amidoamine) dendrimers with supported lipid bilayers and cells: hole formation and the relation to transport. *Bioconjugate Chem.* **2004**, *15*, 774–782.
- (57) Shi, X.; Bányai, I.; Rodriguez, K.; Islam, M. T.; Lesniak, W.; Balogh, P.; Balogh, L. P.; Baker, J. R. Electrophoretic mobility and molecular distribution studies of poly (amidoamine) dendrimers of defined charges. *Electrophoresis* **2006**, *27*, 1758–1767.
- (58) Huang, Q. R.; Dubin, P. L.; Moorefield, C. N.; Newkome, G. R. Counterion binding on charged spheres: Effect of pH and ionic strength on the mobility of carboxyl-terminated dendrimers. *J. Phys. Chem. B* **2000**, *104*, 898–904.
- (59) Böhme, U.; Klänge, A.; Hänel, B.; Scheler, U. Counterion condensation and effective charge of PAMAM dendrimers. *Polymers* **2011**, *3*, 812–819.
- (60) Welch, P.; Muthukumar, M. Tuning the density profile of dendritic polyelectrolytes. *Macromolecules* **1998**, *31*, S892–S897.
- (61) Castagnola, M.; Zuppi, C.; Rossetti, D. V.; Vincenzoni, F.; Lupi, A.; Vitali, A.; Messina, I. Characterization of dendrimer properties by capillary electrophoresis and their use as pseudostationary phases. *Electrophoresis* **2002**, *23*, 1769–1778.
- (62) Shi, X.; Bányai, I.; Lesniak, W. G.; Islam, M. T.; Országh, I.; Balogh, P.; Baker, J. R.; Balogh, L. P. Capillary electrophoresis of polycationic poly (amidoamine) dendrimers. *Electrophoresis* **2005**, *26*, 2949–2959.
- (63) Shi, X.; Majoros, I. J.; Baker, J. R. Capillary electrophoresis of poly (amidoamine) dendrimers: from simple derivatives to complex multifunctional medical nanodevices. *Mol. Pharmaceutics* **2005**, *2*, 278–294.
- (64) Biricova, V.; Laznickova, A. Dendrimers: Analytical characterization and applications. *Bioorg. Chem.* **2009**, *37*, 185–192.
- (65) Shi, X.; Patri, A. K.; Lesniak, W.; Islam, M. T.; Zhang, C.; Baker, J. R.; Balogh, L. P. Analysis of poly (amidoamine)-succinic acid dendrimers by sol-gel electrophoresis and capillary zone electrophoresis. *Electrophoresis* **2005**, *26*, 2960–2967.
- (66) Netz, R. R. Nonequilibrium unfolding of polyelectrolyte condensates in electric fields. *Phys. Rev. Lett.* **2003**, *90*, 128104.
- (67) Netz, R. R. Polyelectrolytes in electric fields. *J. Phys. Chem. B* **2003**, *107*, 8208–8217.
- (68) Shendruk, T. N.; Hickey, O. A.; Slater, G. W.; Harden, J. L. Electrophoresis: When hydrodynamics matter. *Curr. Opin. Colloid Interface Sci.* **2012**, *17*, 74–82.
- (69) Frank, S.; Winkler, R. G. Mesoscale hydrodynamic simulation of short polyelectrolytes in electric fields. *J. Chem. Phys.* **2009**, *131*, 234905.
- (70) Grass, K.; Böhme, U.; Scheler, U.; Cottet, H.; Holm, C. Importance of hydrodynamic shielding for the dynamic behavior of short polyelectrolyte chains. *Phys. Rev. Lett.* **2008**, *100*, 096104.

- (71) Grass, K.; Holm, C. Polyelectrolytes in electric fields: measuring the dynamical effective charge and effective friction. *Soft Matter* **2009**, *5*, 2079–2092.
- (72) Grass, K.; Holm, C. Mesoscale modelling of polyelectrolyte electrophoresis. *Faraday Discuss.* **2010**, *144*, 57–70.
- (73) Hickey, O. A.; Shendruk, T. N.; Harden, J. L.; Slater, G. W. Simulations of Free-Solution Electrophoresis of Polyelectrolytes with a Finite Debye Length Using the Debye-Hückel Approximation. *Phys. Rev. Lett.* **2012**, *109*, 098302.
- (74) Liu, H.; Zhu, Y.; Maginn, E. Molecular Simulation of Polyelectrolyte Conformational Dynamics under an AC Electric Field. *Macromolecules* **2010**, *43*, 4805–4813.
- (75) Wei, Y. F.; Hsiao, P. Y. Unfolding polyelectrolytes in trivalent salt solutions using dc electric fields: A study by Langevin dynamics simulations. *Biomicrofluidics* **2009**, *3*, 022410.
- (76) Wu, K. M.; Wei, Y. F.; Hsiao, P. Y. Polyelectrolytes in multivalent salt solutions. *Electrophoresis* **2011**, *32*, 3348–3363.
- (77) Hsiao, P. Y.; Wei, Y. F.; Chang, H. C. Unfolding collapsed polyelectrolytes in alternating-current electric fields. *Soft Matter* **2011**, *7*, 1207–1213.
- (78) Hsiao, P. Y. Linear polyelectrolytes in tetravalent salt solutions. *J. Chem. Phys.* **2006**, *124*, 044904.
- (79) Hsiao, P. Y. Chain morphology, swelling exponent, persistence length, like-charge attraction, and charge distribution around a chain in polyelectrolyte solutions: effects of salt concentration and ion size studied by molecular dynamics simulations. *Macromolecules* **2006**, *39*, 7125–7137.
- (80) Huißmann, S.; Wynveen, A.; Likos, C. N.; Blaak, R. The effects of pH, salt and bond stiffness on charged dendrimers. *J. Phys.: Condens. Matter* **2010**, *22*, 232101.
- (81) Carrillo, J. M. Y.; Dobrynin, A. V. Polyelectrolytes in salt solutions: molecular dynamics simulations. *Macromolecules* **2011**, *44*, 5798–5816.
- (82) Slater, G. W.; Holm, C.; Chubynsky, M. V.; de Haan, H. W.; Dube, A.; Grass, K.; Hickey, O. A.; Zhan, L. Modeling the separation of macromolecules: A review of current computer simulation methods. *Electrophoresis* **2009**, *30*, 792–818.
- (83) Weeks, D.; Chandler, D.; Andersen, H. C. Role of repulsive forces in determining the equilibrium structure of simple liquids. *J. Chem. Phys.* **1971**, *54*, 5237–5247.
- (84) Kremer, K.; Grest, G. S. Dynamics of entangled linear polymer melts: A molecular-dynamics simulation. *J. Chem. Phys.* **1990**, *92*, 5057–5086.
- (85) Allen, M. P.; Tildesley, D. J. *Computer Simulation of Liquids*; Oxford University Press: New York, 1987.
- (86) Leach, A. R. *Molecular Modeling: Principles and Applications*, 2nd ed.; Pearson Education Limited: Essex, England, 2001.
- (87) Pastor, R. W. Techniques and applications of Langevin dynamics simulations. In *The Molecular Dynamics of Liquid Crystals*; Luckhurst, G. R.; Veracini, C. A., Eds.; Kluwer Academic Publishers: Dordrecht, The Netherlands, 1994; pp 85–138.
- (88) Plimpton, S. Fast parallel algorithms for short-range molecular dynamics. *J. Comput. Phys.* **1995**, *117*, 1–19.
- (89) In our study, the length unit σ is equal to 2.38 Å because the Bjerrum length ($\lambda_B = 3\sigma$) is 7.14 Å in water at 300 K. The energy unit ϵ is equal to 0.02 eV, converted from the setting $k_B T = 1.2\epsilon$. Thus, the unit for electric field $\epsilon/(\epsilon\sigma)$ corresponds to a field strength of 8.4×10^7 V/m in a real system. Consequently, the electric field used in our simulations varies from zero to a strength several orders of magnitude stronger than the field typically applied in experiments. Therefore, the high-field results obtained here should be interpreted with caution.
- (90) The monomer concentration is not fixed against the dendrimer generation because we have fixed the box size in the simulations. The variation of monomer concentration may have an important effect on system properties, particularly on the ion condensation. As presented in Figure 6, nearly all the trivalent salt cations condense on the dendrimers in zero fields. This shows that our monomer concentration is not too dilute to induce unwanted ion decondensation from the dendrimers. The collapse of different physical quantities into master curves in Figure 12 also supports the argument of a weak influence of the variation of monomer concentration in our study. In future studies, more careful simulation setups should be performed to keep the monomer concentration constant by varying the box volume with the dendrimer generation.
- (91) (a) Deserno, M.; Holm, C. How to mesh up Ewald sums. I. A theoretical and numerical comparison of various particle mesh routines. *J. Chem. Phys.* **1998**, *109*, 7678–7693. (b) Deserno, M.; Holm, C. How to mesh up Ewald sums. II. An accurate error estimate for the particle–particle–particle-mesh algorithm. *J. Chem. Phys.* **1998**, *109*, 7694–7701.
- (92) Solc, K. Shape of a Random-Flight Chain. *J. Chem. Phys.* **1971**, *55*, 335–344.
- (93) Arkin, H.; Janke, W. Gyration tensor based analysis of the shapes of polymer chains in an attractive spherical cage. *J. Chem. Phys.* **2013**, *138*, 054904.
- (94) Hsiao, P. Y.; Wu, K. M. Free Solution Electrophoresis of Homopolyelectrolytes. *J. Phys. Chem. B* **2008**, *112*, 13177–13180.
- (95) Yamashita, M.; Kuraoka, K. A method for calculating order parameter and determining orientation direction on polarized molecules in organic–inorganic hybrid film. *J. Mater. Sci.* **2007**, *42*, 2907–2912.
- (96) Wiersema, P. H.; Loeb, A. L.; Overbeek, J. T. G. Calculation of the electrophoretic mobility of a spherical colloid particle. *J. Colloid Interface Sci.* **1966**, *22*, 78–99.
- (97) O'Brien, R. W.; White, L. R. Electrophoretic mobility of a spherical colloidal particle. *J. Chem. Soc., Faraday Trans. 2* **1978**, *74*, 1607–1626.
- (98) Peitzsch, R. M.; Burt, M. J.; Reed, W. F. Evidence of partial draining for linear polyelectrolytes; heparin, chondroitin 6-sulfate, and poly (styrene sulfonate). *Macromolecules* **1992**, *25*, 806–815.
- (99) Walldal, C.; Akerman, B. Effect of ionic strength on the dynamic mobility of polyelectrolytes. *Langmuir* **1999**, *15*, 5237–5243.
- (100) Yue, Y.; Eun, J. S.; Lee, M. K.; Seo, S. Y. Synthesis and characterization of G5 PAMAM dendrimer containing daunorubicin for targeting cancer cells. *Arch. Pharm. Res.* **2012**, *35*, 343–349.
- (101) Nigavekar, S. S.; Sung, L. Y.; Llanes, M.; El-Jawahri, A.; Lawrence, T. S.; Becker, C. W.; Balogh, L.; Khan, M. K. 3H dendrimer nanoparticle organ/tumor distribution. *Pharm. Res.* **2004**, *21*, 476–483.
- (102) Lee, I.; Athey, B. D.; Wetzel, A. W.; Meixner, W.; Baker, J. R. Structural molecular dynamics studies on polyamidoamine dendrimers for a therapeutic application: effects of pH and generation. *Macromolecules* **2002**, *35*, 4510–4520.
- (103) Astruc, D.; Boisselier, E.; Ornelas, C. Dendrimers designed for functions: from physical, photophysical, and supramolecular properties to applications in sensing, catalysis, molecular electronics, photonics, and nanomedicine. *Chem. Rev.* **2010**, *110*, 1857–1959.
- (104) Biswas, P.; Cherayil, B. J. Radial dimensions of startburst polymers. *J. Chem. Phys.* **1994**, *100*, 3201–3209.
- (105) Sadus, R. J. Molecular simulation of dendritic systems. *Mol. Simul.* **2007**, *33*, 569–572.
- (106) Bosko, J. T.; Prakash, J. R. Universal behavior of dendrimer solutions. *Macromolecules* **2011**, *44*, 660–670.